Journal of
Nanoscience and Nanotechnology
Vol. 6, 612–617, 2006

RESEARCH ARTICLE

Growth and Observation of Low-Field Giant Magnetoresistance in $La_{0.7}Sr_{0.3}MnO_3$/ZnO Superlattice Structures

Ashutosh Tiwari[1,*] and J. Narayan[2]

[1] *Nanostructured Materials Research Laboratory (NMRL), Department of Materials Science and Engineering, University of Utah, Salt Lake City, UT 84112, USA*
[2] *NSF Center for Advanced Materials and Smart Structures, North Carolina State University, Raleigh, NC 27695, USA*

We report the growth of a new class of superlattice structure, consisting of alternate layers of $La_{0.7}Sr_{0.3}MnO_3$ (LSMO) and ZnO, which exhibits giant magnetoresistance at low fields. These superlattices were fabricated using a novel pulsed-laser deposition technique with a specially designed target assembly. Giant magnetoresistance of >250% has been observed in these structures in current-in-plane configuration on the application of just ~400 Gauss of magnetic field over the broad temperature range 15–200 K. Observation of giant magnetoresistance at such low magnetic fields is a groundbreaking step in the field of novel magnetic materials and devices.

Keywords: Giant Magnetoresistance, Superlattices, Pulsed Laser Deposition, Interlayer Exchange Coupling.

1. INTRODUCTION

There has been a great surge of interest in materials and devices capable of exhibiting high magnetoresitance. Recent discovery of giant[1–5] magnetoresistance in mixed valence perovkite manganates has been an important milestone in this field. The Double Exchange Interaction[6] (DEI), which involves the hopping of e_g electrons from Mn^{3+} to Mn^{4+} via O^{2-} is understood to be the cause of ferromagnetism and giant magnetoresistive properties of the material. Though the magnetoresistance exhibited by these oxides is quite huge, it requires large magnetic field, typically of the order of few Tesla, making these materials impractical for direct application in actual magnetic devices. In order to have any practical application it is desirable to have materials or devices, which can exhibit Low field magnetoresistance (LFMR).

Recently artificially structured superlattice structures[7,8] consisting of ferromagnetic (FM) layers separated by nonmagnetic (NM) layers have attracted significant attention for LFMR applications. Interlayer exchange coupling[9] (IEC) between the ferromagnetic layers determines the overall characteristics of the structure. The IEC can be ferromagnetic or antiferromagnetic depending upon the nature of the magnetic ordering in the film, nature of the nonmagnetic buffer layer, and its thickness. The IEC across metallic interlayer shows a damped oscillation between the ferromagnetic and antiferromagnetic states as a function of interlayer spacing due to the formation of standing electron waves in the interlayer.[10] On the other hand for insulating spacer layers, there are only evanescent waves, which decay very fast as the distance from the interface increases, and hence the IEC in these structures is very week. In the structures with semiconducting interlayers, the strength of IEC is expected to lie in between that of metal and insulator.

It has been shown[2,11] that FM-NM-FM multilayer structures, with anti-ferromagnetic interlayer exchange coupling exhibit giant tunneling magnetoresistance in out-of-plane direction. In the absence of any magnetic field, magnetic layers are aligned antiferromagnetically, and it corresponds to a high resistive state. When a sufficiently strong magnetic field is applied, it tries to align the individual FM aligned layers parallel to the field. Ferromagnetically aligned configuration is a low resistance state. So a shift from an AFM aligned state to a FM aligned state results in a large magnetoresistance. The strength of the magnetic field required to do this transformation depends on the strength of IEC. If the strength of IEC is weak then ferromagnetic layers will be feebly aligned and even a small magnetic field will be sufficient to cause a transition

*Author to whom correspondence should be addressed.

1533-4880/2006/6/612/006 doi:10.1166/jnn.2006.118

from high resistance AFM aligned state to low resistance FM configuration.

Low values of IEC can be realized by using insulating or semiconducting interlayers.[10] However, in the case of good insulators IEC is predicted to be vanishingly small and in this kind of situation because of the thermal excitation energy magnetic layers may lose their out-of-plane magnetic ordering completely. In the case of semiconductors the strength of IEC lies between that of metals and insulators, hence they can give rise to optimum strength of IEC to realize LFMR. We envisaged that ZnO may be a suitable material for this application when used in conjunction with ferromagnetic LSMO layers. ZnO is a wide band gap ($E_g = 3.3$ eV) semiconductor[12] but still possesses significant electrical conductivity. Because of this unique characteristics, ZnO is expected to result in a small but still nonzero IEC in LSMO/ZnO superlattice structures. However, since ZnO and LSMO have completely different crystal structure with a lattice mismatch (ZnO is hexagonal while LSMO has cubic perovskite structure) it presents a significant challenge to grow epitaxial superlattice structures consisting of these materials. Probably because of the above perception so far no efforts have been made to grow any such heterostructured superlattice. However, recently a new concept[13] of "Domain Matching Epitaxy" (DME) has emerged in which a large lattice mismatch can be accommodated by the matching of integral multiples of lattice plane across the film-substrate interface. If the lattice mismatch lies in between the integral multiples, two domains alternate with a certain frequency according to the principle[13] of domain variation to achieve zero residual misfit. Inspired by the DME approach we have prepared LSMO/ZnO superlattice structures which have shown exciting new results. Here we are reporting our results on the growth and observation of giant LFMR in ZnO/LSMO superlattice structures.

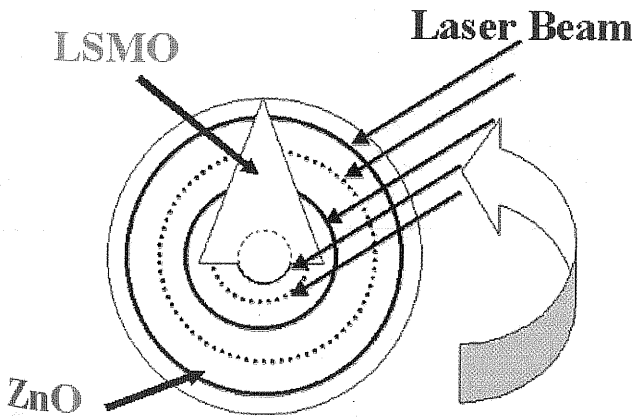

Fig. 1. Schematic diagram showing the arrangement of ZnO and LSMO targets for the growth of ZnO/LSMO superlattices.

2. EXPERIMENTAL DETAILS

These structures were grown by pulsed laser deposition technique with LSMO and ZnO targets arranged in a special geometry (see Fig. 1). Laser pulses from a KrF excimer laser (Lambda Physik 210, $\lambda = 248$ nm) were made incident on the target assembly at an angle of 45° from the normal. Target assembly was rotating on its own axis with an angular velocity of 18°/s. This specially configured rotating target assembly facilitates the continuous ablation of LSMO and ZnO one after the other in a precise and controlled way. Relative thickness of individual layers depends on the relative time of ablation of materials, and their respective ablation rates. Relative time of ablation was controlled by changing the relative area of substrates. Ablation rate of LSMO and ZnO was determined separately as a function of laser energy density. For the laser energy density of 4 J/cm^2 the rate of ablation of ZnO and LSMO were 0.6 Å/pulse and 0.4 Å/pulse, respectively. It took about 20 seconds to fabricate one pair of ZnO/LSMO layer with the laser pulse repetition rate of 10 Hz and in just 15 minutes we were able to fabricate superlattice structure with more than 45 layers of ZnO and LSMO each.

3. RESULTS AND DISCUSSION

Figure 2(a) shows the low-angle X-ray scattering data (LAXRD) of LSMO/ZnO superlattice. In the 2θ angle range of 5–10° we observed seven peaks, indicating a strong composition modulation along the growth direction. The value of bilayer period Λ was determined to be 13.5 ± 0.5 nm by fitting the XRD peaks in the relation:[14, 15] $\sin^2(\theta) = (n\lambda/2\Lambda)^2 + 2\delta_s$; in this equation '$2\theta$' is the angle of diffraction, 'n' is the order of diffraction, 'λ' is the wavelength of CuK_α radiation and 'δ_s' is a small dimensionless constant ($\sim 3 \times 10^{-5}$). High-angle X-ray diffraction data (HAXRD) from the superlattice structure is shown in Figure 2(b). In the angle range of 20–100 we observed peaks corresponding to (0002) and (0004) planes of ZnO; (111) and (222) planes of LSMO; and (0006), (00012) planes of sapphire substrate. A cursory look at the high angle X-ray data shows that c-axis of ZnO in these structures is aligned parallel to $\langle 111 \rangle$ direction of LSMO which is perpendicular to the (0001) plane of sapphire substrate. Observation of individual peaks for ZnO and LSMO points towards the large thickness of bilayers (>10 nm). In the case of ZnO(0002) peaks, two additional satellite peaks, characteristics of superlattices, on either side of the main peak were observed. By using the position of this peak and its satellite peaks in the equation:[14, 15] $2\sin(\theta)/\lambda = 1/d \pm n/\Lambda$; we estimated the value of Λ as 13.0 ± 0.5 nm, which is in excellent agreement with the value obtained from LAXRD data.

ZnO/LSMO superlattices were further characterized using STEM Z-contrast and HRTEM. Figure 3(a) shows

RESEARCH ARTICLE

a STEM (Z contrast) image of the ZnO/LSMO superlattice on Sapphire. In STEM Z-contrast spectroscopy[16] the contrast of the STEM image is proportional to Z^2. Since the atomic number of La and Sr are much larger than that of Zn. The LSMO layers have a brighter contrast compared to ZnO. Inset of this figure shows the STEM image of ZnO/LSMO superlattice structure with a higher magnification. Long-range periodic structure with structural coherence and sharp interfaces of ZnO/LSMO can clearly be visualized. The total thickness of the superlattice structure in this sample is about 500 nm, which corresponds to 45 bilayers of LSMO (5 nm) and ZnO (6 nm). In order to further characterize the microstructure and to determine the orientational relationship between different layers we performed High Resolution TEM (HRTEM) and selected area electron diffraction (SAED) measurements. Figures 3(b) and (c) show HRTEM image and SAED pattern of LSMO/ZnO superlattice in the $[01\bar{1}0]$ direction of sapphire. As a result of a detailed analysis of this diffraction pattern we obtained following epitaxial relationship between different layers: $[\bar{1}11]_{LSMO}||[0001]_{ZnO}||[0001]_{Sapphire}$; $[01\bar{1}0]_{ZnO}||[2\bar{2}4]_{LSMO}||[\bar{2}110]_{Sapphire}$. In this configuration five $[03\bar{3}0]$ planes of ZnO match with six $[2\bar{2}4]$ planes of LSMO within the framework of domain matching epitaxy.[13]

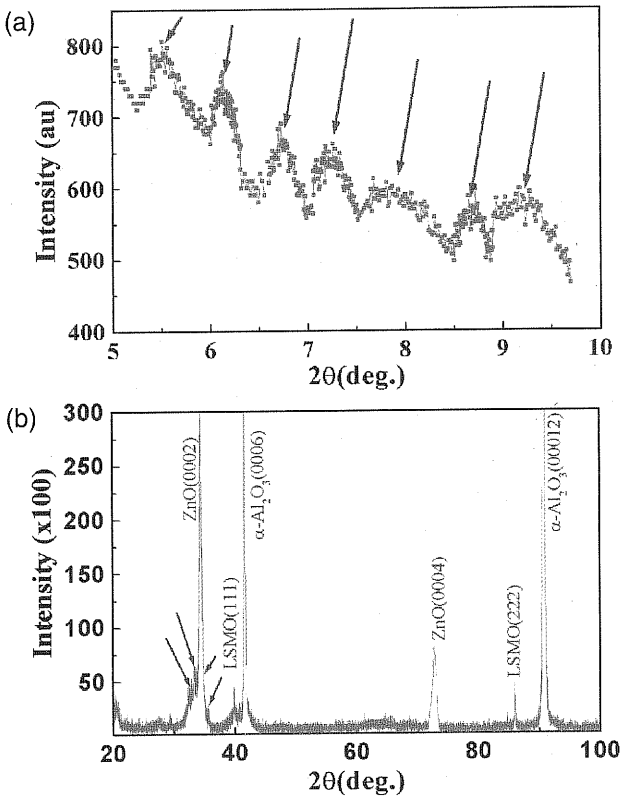

Fig. 2. X-ray diffraction data from LSMO/ZnO superlattice. (a) Low-angle X-ray diffraction pattern. Arrows indicate LAXRD peaks. (b) High-angle X-ray diffraction pattern. Arrows around ZnO(0002) peak represent satellite peaks.

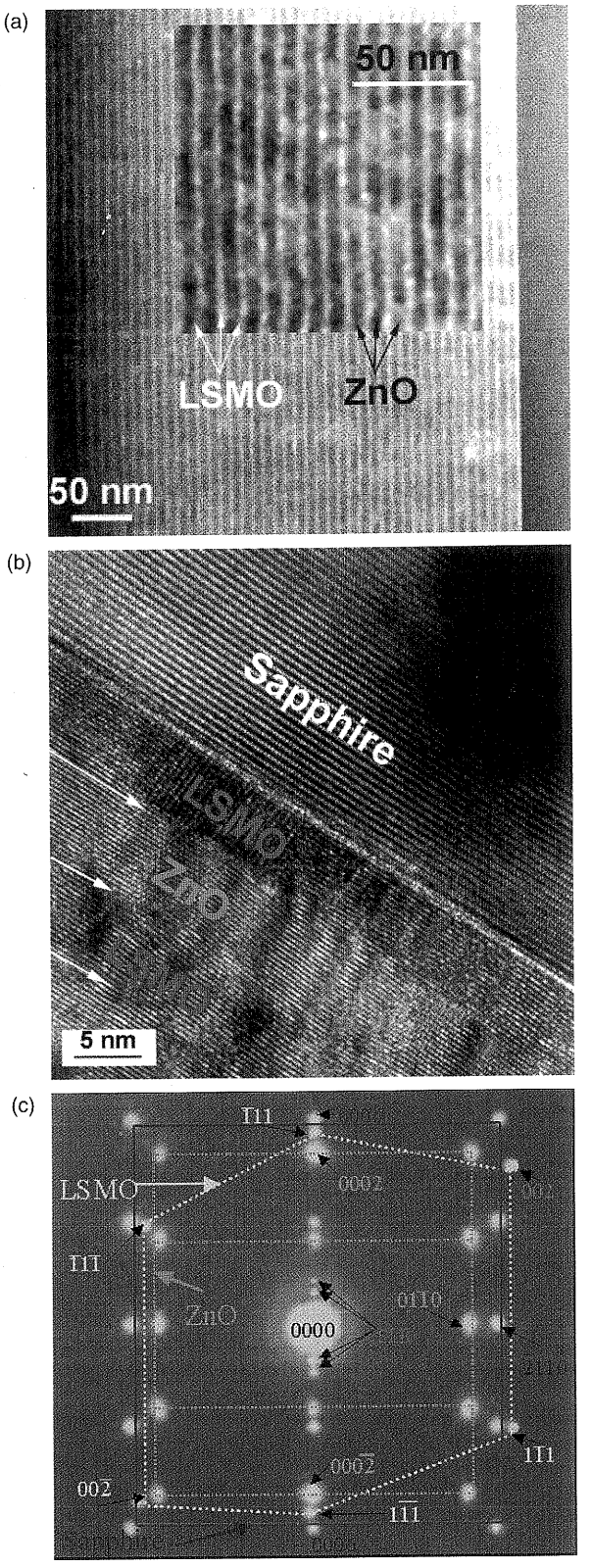

Fig. 3. TEM micrographs and SAED from LSMO/ZnO superlattice. (a) STEM Z-contrast image in the $[01\bar{1}0]$ direction of sapphire. Inset shows a part of this image with a higher magnification. (b) HRTEM image in the $[01\bar{1}0]$ direction of sapphire; and (c) Selected area electron diffraction pattern showing spots corresponding to ZnO, LSMO, and sapphire.

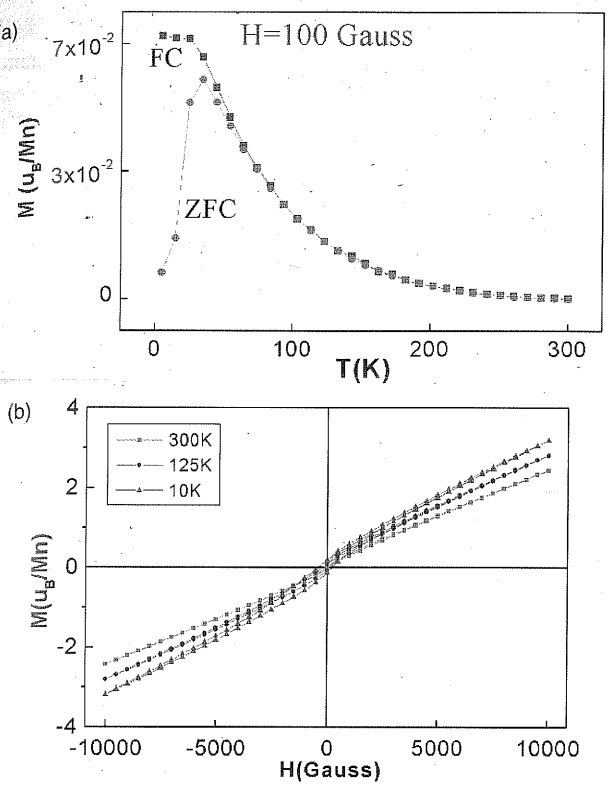

Fig. 4. Magnetization data of ZnO/LSMO superlattice. (a) Magnetization vs Temperature, and (b) Magnetization vs Field at different temperatures.

Magnetic measurements on ZnO/LSMO superlattice were made using Quantum Design Squid Magnetometer. Figure 4(a) shows magnetization data as a function of temperature on the application of a small field of 100 Gauss parallel to the plane of the substrate. ZFC and FC magnetization data exhibit significant deviation at lower temperatures. Deviation of ZFC and FC magnetization curves is an indication of over-all superparamagnetic nature of the material. M vs H characteristics at 10 K, 125 K, and 300 K are shown in Figure 4(b). M vs H data at 10 K and 125 K show a nonlinear behavior with coercivity ~180 Gauss and ~150 Gauss, however, it shows no signature of saturation even upto 1 T of field. This suggests the antiferromagnetic arrangement of LSMO layers in the out-of-plane direction. M vs H at 300 K, also shows a slight nonlinear behavior but with almost zero coercivity in accordance with the super-paramagnetic behavior of the system. Here it is to be noted that the ferromagnetic Curie temperature of bulk LSMO is 360 K.[17] But since in our superlattices LSMO layers are just few nanometer thick and they are separated by nonmagnetic semiconducting ZnO layers, thermal energy at higher temperature may be sufficient to randomize the magnetic moments in out-of-plane direction and it may be the cause of the observed superparamagnetic characteristic of the magnetization data.

Electrical resistance of ZnO/LSMO superlattices in out-of-plane and in-plane configurations, are shown in

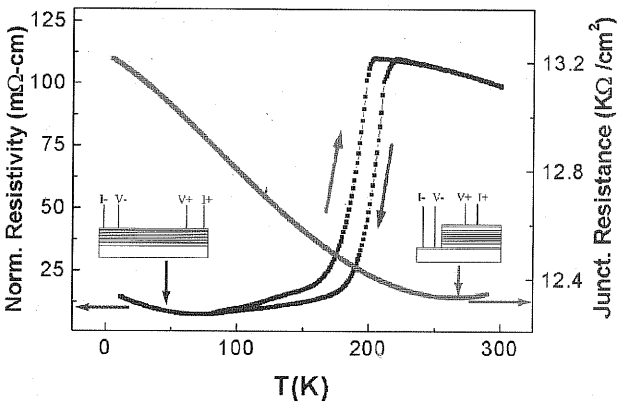

Fig. 5. Electrical resistance data for LSMO/ZnO superlattice. Left *y*-axis is for in-plane configuration and right for out-of-plane configuration. The in-plane resistivity data was obtained by normalizing the in-plane resistance data by the total thickness of LSMO layer. The out-of-plane electrical data was normalized by the effective junction area (2×2 mm^2). Insets show the measurement geometry.

Figure 5. Specimen for out-of-plane resistivity measurement was prepared by masking a 2×2 mm^2 area of SL by a thick metal sheet and exposing the unmasked area by ultra high power laser pulses to remove all the layers except the bottom LSMO layer (see inset in Fig. 5). All the measurements were performed using four-point-probe technique. In the out-of-plane configuration resistance of LSMO and ZnO layers are arranged in a series configuration and hence the net resistance of the system is the sum of individual contributions from ZnO and LSMO. Since ZnO has higher resistance, it determines overall out-of-plane resistance and hence ZnO/LSMO superlattice exhibit semiconductor kind of temperature dependence. In contradiction to this in-plane electrical resistance data shows much more interesting features. It undergoes a metal-insulator transition as a function of temperature with insulating behavior at high temperature and metallic behavior at low temperature. Most intriguing feature of electrical resistivity data is the observation of significant thermal hysteresis near T_{M-I}. Hysteresis is usually observed in first order phase transitions but the directions of hysteresis in these transitions are exactly opposite to what has been encountered in our samples. The cause of this strange and intriguing observation is not clear yet, but we believe that this may have its origin in the temperature dependent changes in the linear expansion coefficient of LSMO. In a recent paper, Rivadulla et al.[18] have reported a hysteretic temperature dependence of thermal expansion of LCMO. This hysteresis in the thermal expansion will result in the same resistance hysteresis direction as observed in our case.

Magnetoresistive response of the system was checked by applying a small field of ~400 Gauss. When this magnetic field is applied, temperature dependence of the out-of-plane resistance remains almost same but its magnitude decreases by a small amount, giving rise to a small negative magnetoresistance of about 0.5%. On the other

hand, in the case of in-plane resistance, T_{M-I} shifts to lower temperature by about 100 K giving rise to huge positive magnetoresistance (>250%) over the wide temperature range 15–200 K. Though the small and negative magnetoresistance in out-of-plane orientation can easily be ascribed to characteristic behavior of LSMO, the huge positive magnetoresistance in in-plane direction is really amazing and has tremendous potential for applications in magnetic devices. We believe that the following two factors are responsible for the unique LFMR characteristics of ZnO/LSMO SL structures: (i) low values of IEC due to the semiconducting behavior of ZnO and (ii) DME growth mode of ZnO/LSMO structure. In the DME framework,[13] it is possible to grow better quality (lower dislocation density) thin films at larger lattice misfit compared to smaller lattice misfit, where dislocations nucleate on the surface as half loops and create threading dislocations. In highly mismatched systems like ZnO/LSMO, the critical thickness is about one monolayer, so most of the dislocations set from the beginning and rest of the layer grows strain free.

Here we find it essential to mention that the observed LFMR characteristic of LSMO/ZnO superlattice structure is entirely different from the one usually observed in other superlattice structures.[10, 20] In the later systems the sign of MR is negative and it requires significantly high fields. Applied magnetic field should be sufficiently strong (of the order of saturation field, H_S) to change the configuration of magnetic layers from antiferromagnetically aligned state to ferromagnetically aligned state.[19, 20] In contrary to this ZnO/LSMO multilayers show giant magnetoresistance at field values which are much smaller than the H_S. This suggests the possibility of an entirely new physical phenomenon, responsible for the observed giant LFMR in ZnO/LSMO superlattices. Here we discuss a plausible mechanism (see Fig. 6), which may explain the observed LFMR in ZnO/LSMO superlattices. This mechanism involves a delicate balance between in-plane double exchange interaction and out-of-plane interlayer exchange coupling and electron tunneling. In the absence of field, layers are antiferromagnetically aligned [See Fig. 6a], so conduction electrons are confined in individual layers and are responsible for the in-plane double exchange interaction in these layers. When a magnetic field is applied, it tends to align magnetic moments of individual LSMO layers parallel to each other [See Fig. 6b]. However, if the strength of applied field is small, it may not be able to align the magnetic layers completely parallel to each other but still it can change the angle between the magnetization vectors of adjacent layers from 180° to less than 180°, this will slightly enhance the probability of quantum mechanical tunneling of electrons between adjacent LSMO layers in out-of-plane direction. Under this situation, electrons will be less available for contributing to double exchange interaction inside the individual layers. Since in manganates, the strength of DEI is very sensitive to effective carrier concentration; even a slight decrease in the carrier concentration may lead to significant reduction in the strength of DEI. Because of the reduced double exchange interaction, thermal energy will dominate and randomize the spin orientation resulting in a decrease in the metal-insulator transition temperature and consequently resulting in the phenomenon of giant low field magnetoresistance.

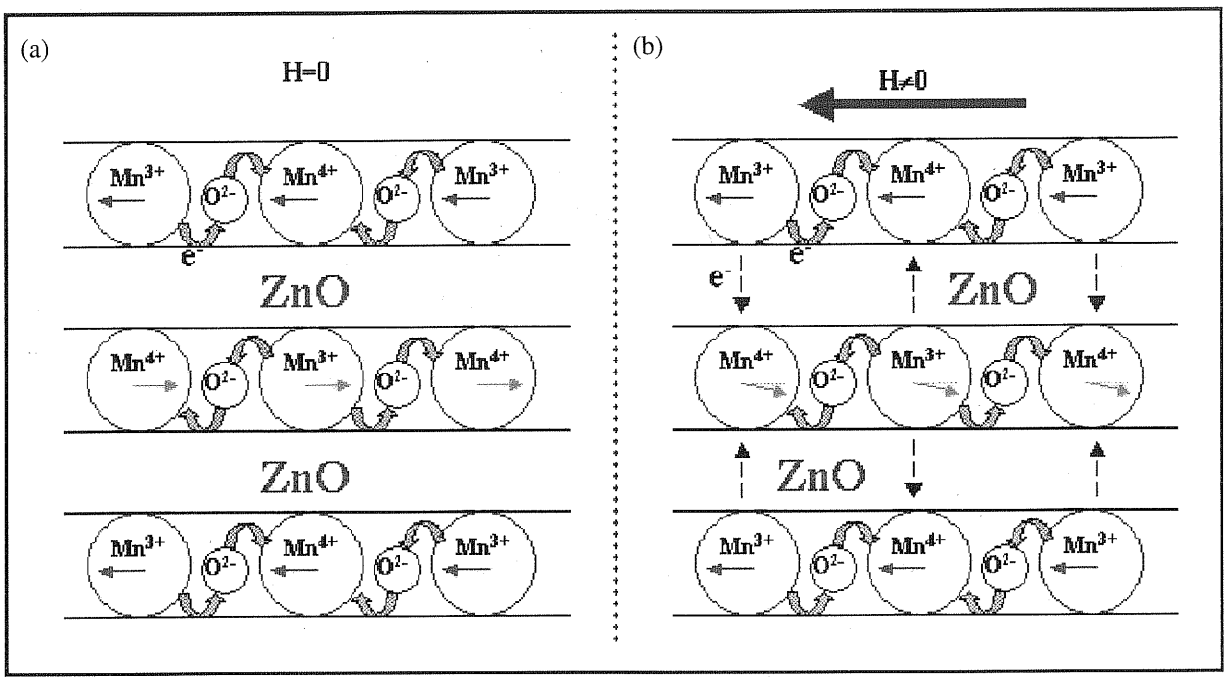

Fig. 6. Schematic diagram illustrating the spin configuration of different LSMO layers. (a) with out magnetic field and (b) with magnetic field.

4. CONCLUSIONS

Finally we conclude this article by stating that we have observed giant low field magnetoresistance in ZnO/LSMO superlattice structure. A huge low field magnetoresistance of more than 250% has been observed over a very broad temperature range 15–200 K with a maximum of about 1100% at ~100 K on the application of just 400 Gauss of magnetic field. A delicate interplay between in-plane double exchange interaction and out-of-plane interlayer exchange coupling between adjacent LSMO layers is understood to be the cause of giant LFMR. ZnO interlayers play the key role in these structures by providing the optimum value of IEC strength, which is critical for the realization of LFMR. Observation of giant low field magnetoresistance at such low magnetic fields and over such a broad temperature range is a landmark step in the field of magnetic materials. This work becomes of special significance because of recent developments in the field of ultra-high capacity magnetic storage devices.[21] Efforts are going on to prepare systems based on similar principles for room temperature LFMR applications.

Acknowledgments: Authors want to thank Dr. John T. Prater (Army Research Office) and Dr. A. K. Majumdar (I.I.T. Kanpur) for very useful discussions.

References and Notes

1. S. Jin, T. H. Tiefel, M. McCormack, R. A. Fastnacht, R. Ramesh, and L. H. Chen, *Science* 264, 413 (**1994**).
2. J. Z. Sun, W. J. Gallagher, P. R. Duncombe, L. Krusin-Elbaum, R. A. Altman, A. Gupta, Yu Lu, G. Q. Gong, and Gang Xiao, *Appl. Phys. Lett.* 69, 3266 (**1996**).
3. S. S. P. Parkin, N. More, and K. P. Roche, *Phys. Rev. Lett.* 64, 2304 (**1990**).
4. V. Moshnyaga, B. Damaschke, O. Shapoval, A. Belenchuk, J. Faupel, O. I. Lebedev, J. Verbeeck, G. Van Tendeloo, M. Mucksch, V. Tsurkan, R. Tidecks, and K. Samwer, *Nature Mater.* 2, 247 (**2003**).
5. Meon-Ho Jo, N. D. Mathur, N. K. Todd, and M. G. Blamire, *Phys. Rev. B* 61, R14905 (**2000**).
6. C. Zener, *Phys. Rev. B* 82, 403 (**1951**); C. Zener, *Phys. Rev. B* 81, 440 (**1951**).
7. I. K. Schuller, S. Kim, and C. Leighton, *J. Magn. Magn. Mater.* 200, 571 (**1999**).
8. K. R. Nikolaev, A. Yu. Dobin, I. N. Krivorotov, W. K. Cooley, A. Bhattacharya, A. L. Kobrinskii, L. I. Glazman, R. M. Wentzovitch, E. Dan Dahlberg, and A. M. Goldman, *Phys. Rev. Lett.* 85, 3278 (**2000**).
9. M. D. Stiles, *J. Magn. Magn. Mater.* 200, 322 (**1999**).
10. D. E. Burgler, M. Buchmeier, S. Cramm, S. Eisebitt, R. R. Gareev, P. Grunberg, C. L. Jia, L. L. Pohlmann, R. Schreiber, M. Siegel, Y. L. Qin, and A. Zimina, *J. Phys.: Condens. Matter* 15, S443 (**2003**).
11. M. N. Baibich, J. M. Broto, A. Fert, F. Nguyen Van Dau, F. Petroff, P. Eitenne, G. Creuzet, A. Friederich, and J. Chazelas, *Phys. Rev. B* 61, 2472 (**1988**).
12. H. Ohno, *Science* 281, 951 (**1998**).
13. J. Narayan, U.S. Patent 5,406,123 (**1995**); J. Narayan and B. C. Larson, *J. Appl. Phys.* 93, 278 (**2003**).
14. P. F. Miceli, D. A. Neumann, and H. Zabel, *Appl. Phys. Lett.* 48, 24 (**1986**).
15. E. E. Fullerton, I. K. Schuller, H. Vanderstraeten, and Y. Bruynseraede, *Phys. Rev. B* 45, 9292 (**1992**).
16. S. Lopatin, S. J. Pennycook, J. Narayan, and G. Duscher, *Appl. Phys. Lett.* 81, 2728 (**2002**).
17. A. Tiwari and K. P. Rajeev, *Phys. Rev. B* 60, 10591 (**1999**).
18. F. Rivadulla, L. E. Hueso, D. R. Miguenes, P. Sande, A. Fondado, J. Rivas, M. A. Lopez-Quintela, and C. A. Ramos, *J. Appl. Phys.* 91, 7412 (**2002**).
19. S. S. P. Parkin, Z. G. Li, and D. J. Smith, *Appl. Phys. Lett.* 58, 2710 (**1991**).
20. R. Schad, C. D. Potter, P. Beliën, G. Verbanck, V. V. Moshchalkov, and Y. Bruynseraede, *Appl. Phys. Lett.* 64, 3500 (**1994**).
21. J. Narayan and A. Tiwari, *J. Nanosci. Nanotechnol.* 4, 726 (**2004**).

Received: 4 November 2005. Revised/Accepted: 11 November 2005.